Dynamic Response of Shallow-Buried Tunnels Traversing High Loess Slopes

SUN Wen[1,2,3], LIANG Qingguo[1,2]*, WANG Lili[4] and CAO Xiaoping[2]

1）National Demonstration Center for Experimental Civil Engineering Education, Lanzhou Jiaotong University, Lanzhou 730070, China
2）School of Civil Engineering, Lanzhou Jiaotong University, Lanzhou 730070, China
3）Gansu Architectural Science Research Institute Co., Ltd., Lanzhou 730070, China
4）Key Laboratory of Loess Earthquake Engineering of China Earthquake Administration, Lanzhou 730000, China

Considering the existence of numerous shallow-buried tunnels traversing high slopes in the loess area in western China and the fact of high seismic intensity there, we investigate the dynamic response rules of a shallow-buried loess tunnel and its slope under the action of seismic waves with different intensities. Through large-scale shaking table model tests, we successfully analyze the characteristics and process of the destabilization of tunnels and slopes, and propose valuable suggestions regarding the reinforcement parts of a tunnel for reducing seismic damage. The results show that the main seismic damage on a slope include the failure of the sliding surface between the top and foot and the stripping of the soil around the tunnel entrance, while the damage on a tunnel is mainly manifested as the seismic-induced subsidence at the portal section and the cracking deformation at the joint areas. Finally, we propose that the "staggered peak distribution" phenomenon of the maximum acceleration values at the vault and inverted arch area can be considered as a criterion indicating that the tunnel enters into the threshold of dynamic failure.

Key words：Loess; High slope; Shallow-buried tunnel; Dynamic response

INTRODUCTION

　　Compared with the effect on ground structures, the seismic damage on a tunnel is

relatively slight due to the restraint of surrounding rock (Hashash Y.M.A. et al., 2001). However, through the investigation of mountain tunnels from the 1999 Chichi earthquake to the 2008 Wenchuan earthquake, it is found that a large number of tunnels have been damaged in varying degrees under the action of earthquakes (Guo Zihong et al., 2019; Zhang Hong et al., 2016). The portal section of shallow buried tunnels and the geologically complicated tunnel body sections are the concentrated parts where seismic damage occurs (Wang W.L. et al., 2001; Wang Zhengzheng et al., 2009). The extent of tunnel damage in the epicenter is closely related to its buried depth. The real seismic damage data show that a rock tunnel buried more than 50 m will have a significantly lower seismic damage degree (Li Tianbin, 2008; Jiang Shuping et al., 2014). The Loess Area in Western China is an earthquake-prone zone. In recent years, with the advance of "the Belt and Road" policy in China, the traffic construction in the loess area has developed rapidly. However, the requirements of road line direction and elevation setting in such an area with abundant gullies have inevitably led to the connection between high bridges and high tunnels, resulting in numerous shallow-buried tunnels traversing high slopes. The dynamic stabilityin the portal section of a shallow buried loess tunnel reflects the overall seismic capacity of the tunnel. To date, numerous investigations regarding high slope tunnels have been conducted, including dynamic response characteristics, dynamic failure forms, seismic measures, dynamic stability analysis, etc. In particular, Liang Qingguo et al. (2018) studied the dynamic response variation rules and dynamic stability influencing factors of tunnels traversing loess side slopes under the effect of earthquakes (Wang Lili et al., 2016). Jiang Yitao et al. (2016) studied the dynamic response characteristics and seismic measures of shallow-buried tunnels (Geng Ming, 2014; Li Xiaoyun, 2011; Yuan Shuai, 2008; Zhu Yongsheng, 2006). Jiang Shuping et al. (2014) analyzed the seismic response of mountain tunnels with different buried depths (Li Lin et al., 2011). Most of the previous studies focused on the typical cases in which the tunnel was located at the bottom of the slope, but only a handful of investigations have studied the dynamic influence rules and seismic performance of the shallow buried tunnel at the portal section of high loess slopes.

This paper selects a typical shallow-buried loess tunnel on Baoji-Lanzhou highway as the research object. Based on the above analysis combined with large-scale shaking table model tests, we analyze the response rules of the shallow-buried loess tunnel and slope under the action of seismic waves with different intensities, including acceleration response, dynamic soil pressure response, and the destruction on tunnels and slopes. Finally, we propose the destabilization mechanism of shallow-buried loess tunnels, for the purpose of providing a reference for earthquake protection in the loess area.

1 MODEL DESING

Taking a large cross-section of the loess tunnel on Baoji-Lanzhou highway as the research object, the prototype tunnel diameter is $d = 13$ m, the slope height is $h = 117$ m, the slope gradient is $\alpha = 45°$, and the buried depth is $h = 39$ m (the tunnel enters at 1/3 height of the elevation). Considering the size of shaking table and model box, the model slope height is 144 cm, the slope gradient $\alpha = 45°$ and the tunnel is at 1/3 height of the elevation. The buried depth of the model tunnel is 50 cm and the length is 100 cm. The similarity ratio of the surrounding rock in model test is shown in Table 1.

Table 1　Similarity ratio of the surrounding rock parameters in model test

Physical quantity	Similarity relation	Similarity ratio
Length	C_L	80
Time	C_t	1
Elastic modulus	C_E	80
Mass density	C_ρ	1
Acceleration	C_a	1

1. 1　Model Materials

The model tests are conducted on a large-scale electric servo seismic shaking table of Lanzhou Institute of seismology, CEA. The length × width × height of the model box is 2. 8 m×1. 4 m×1. 9 m. In order to reduce the boundary influence induced by the "model box effect" and increase the frictional resistance at the bottom of the model, a flexible polyethylene foam board is installed inside the width direction of the model box. In addition, pebbles with diameters of about 3−5 cm are laid at the bottom of the model box and bonded with cement mortar.

Considering that the prototype loess cannot meet the requirements of the similarity law, the model soil sample we select have a density similarity ratio $C_\rho = 1$. On this basis, we conduct the dynamic triaxial tests on different proportion schemes. Finally, it is determined that the model soil is composed of Q_3 loess, barite powder, sawdust and water. The ratio of each material is: loess (undisturbed): Barite powder: sawdust (passing 0. 5 mm sieve): water = 0. 835 : 0. 04 : 0. 015 : 0. 11. The main physical properties of the prototype soil and model soil are shown in Table 2.

Table 2　Comparison of physical properties of materials

Sample type	water content $\omega/\%$	Density $\rho_d/(g/cm^3)$	Cohesion C/kPa	internal friction angle $\varphi/(°)$
Prototype soil	11	1. 5	22. 40	29. 80
Model soil	11	1. 5	25. 13	30. 01

Prior to the filling step, all kinds of materials are fully mixed and sealed for 24 hours. The model adopts the method of layered filling and manual compaction, in which each layer is about 30 cm, and the compaction degree is controlled according to $D_C = 0. 95$. After the filling step of each layer, the cutting ring method is used to detect the dry density and water content to ensure the filling quality.

The cross section of the tunnel model is simplified as a circle, and the lining thickness of the model is 2 cm. In order to simulate the actual state of the tunnel, such as expansion joint and settlement joint, the tunnel model is spliced by two sections. In the tunnel model, the wire mesh with a diameter of 0. 8 mm is used to simulate the reinforcement framework, and the micro concrete is used as the aggregate. The gravel with larger particle size (2−5 mm) is used as the aggregate to replace the crushed stone in the concrete. Its mechanical

properties and gradation structure are similar to those of ordinary concrete; thus, it is an ideal model test material (Lou Kangyu, 1988). The results show that the mixing ratio of micro concrete of the tunnel model is cement : water : fine sand = 1 : 1.1 : 5.4, and the average compressive strength is 5.28 MPa, which meets the similar ratio requirements of the prototype (C_{30}) concrete.

1.2   Layout of Monitoring Instruments

In the model, 25 acceleration sensors and 12 soil pressure sensors are mainly arranged. The acceleration sensors are mainly distributed evenly along the slope and around the tunnel, and the soil pressure are evenly arranged at the contact position between the vault and inverted arch of the tunnel. The sensors are embedded in the filling process, and the transmission line is fixed on the model box to avoid the swing effect on data acquisition accuracy. During the experiment, the varying characteristics of the model are recorded by high-speed camera. The sensor distribution is shown in Fig.1.
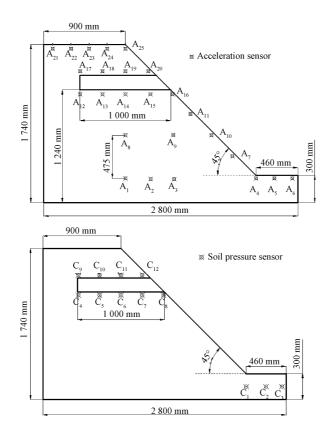

Figure 1   Arrangement of monitoring point

1.3   Loading Condition

Wenchuan Tangyu wave and El-Centro wave after baseline correction are selected for model test. The loading waveform and Fourier spectrum are shown in Fig.2.

The combination of excitation direction is X-direction (horizontal and longitudinal

direction of tunnel）and joint loading of *X*-direction and *Z*-direction（horizontal and vertical direction of tunnel）. The vibration intensity is from weak to strong，and the loading process is conducted according to 15 working conditions listed in Table 3 until the whole model is destroyed.
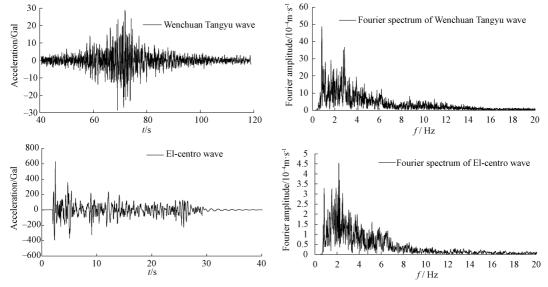

Figure 2　Loading waveform

Table 3　Test loading conditions

Conditions GK	Wave form	Loading direction	Corresponding basic intensity	PGA /Gal	Conditions GK	Wave form	Loading direction	Corresponding basic intensity	PGA /Gal
1	Wenchuan-Tangyu wave	one-way *X*		*X*:116	9	Wenchuan-Tangyu wave	one-way *X*		*X*:465
2	Wenchuan-Tangyu wave	two-way *X/Z*	7	*X*:116 *Z*:78	10	Wenchuan-Tangyu wave	two-way *X/Z*	9	*X*:465 *Z*:312
3	El-Centro wave	one-way *X*		*X*:117	11	El-Centro wave	one-way *X*		*X*:470
4	El-Centro wave	two-way *X/Z*		*X*:117 *Z*:54	12	El-Centro wave	two-way *X/Z*		*X*:470 *Z*:215
5	Wenchuan-Tangyu wave	one-way *X*		*X*:233	13	Wenchuan-Tangyu wave	one-way *X*		*X*:698
6	Wenchuan-Tangyu wave	two-way *X/Z*	8	*X*:233 *Z*:156	14	sine sweep	one-way *X*	Over 9	*X*:50
7	El-Centro wave	one-way *X*		*X*:235	15	Wenchuan-Tangyu wave	two-way *X/Z*		*X*:698 *Z*:468
8	El-Centro wave	two-way *X/Z*		*X*:235 *Z*:107					

2　ANALYSIS OF MODEL FAILURE CHARACTERISTICS

From GK_1 to GK_{15} , the input seismic wave intensity increases gradually until the whole

model is destroyed. Due to the influence of boundary effect，cracks initially appear at the top of the slope，and then shear transverse cracks occur at the foot of the slope. With the increase of the input seismic wave intensity，a large number of irregular cracks appear on the slope around the portal section of the tunnel. With the further development of the cracks，the entire slope slides down. The typical destabilization characteristics of the model are consistent with the seismic damage of the mountain-traversing tunnels and high loess slopes under actual seismic conditions（Wang Lanmin et al.，2019；Wang Mingnian et al.，2012）. According to the damage severity and failure characteristics of the model，the failure processis divided into the following four stages：stable stage，loose body stripping stage，local damage development stage and overall instability failure stage. The specific analysis is shown in Table 4：

Table 4　Stage of deformation and failure for model

Sequence number	Stage	Corresponding conditions GK	Main failure modes and analysis
①	Stable stage	1-4	The model does not change significantly
②	Loose body stripping stage	5-8	There are two cracks at the boundary of the top of the slope，a small amount of soil falls on the slope surface，and a vertical crack with a length of 25 cm appears on the right side of the top slope. In this stage，the seismic wave affects the weak position of the soil structure，and the original limit equilibrium state is destroyed，causing the falling or stripping of the loose soil. However，it has little impact on the overall strength and stability of the slope and its structure.
③	Development stage of local earthquake damage	9-13	First of all，1. 5-2 cm seismic subsidence occurs at the rear boundary of the top slope，and the lateral shear cracks appear at the slope toe，exhibiting shear-out trend. Then，the cracks on the top of the slope extend to the slope surface，and the maximum seismic subsidence depth reaches 5. 5 cm. The transverse cracks on the slope toe are widened，and finally，the cracks at the top and foot of the slope are connected together，forming a collapse zone. At this stage，some failures appear in the soil of the slope and several underground structures，influencing their strength and stability. With the further accumulation of failure，the model reaches the threshold of the overall failure.
④	Whole failure stage	15	The soil mass at the top of the slope slides entirely，a large amount of soil falls down. The portal section of the tunnel slides down 9 cm，and the whole slope surface slides along the side arc through cracks，forming an obvious sliding surface.

In the four stages of model failure process，the transition process from ② to ③ is

relatively unclear compared with that from ① to ②, ③ to ④. The failure modes of each stage are shown in Fig.3− Fig.5.

3   ANALYSIS ABOUT ACCELERATION RESPONSE

In order to improve the pertinence and continuity of the analysis, the double-sided (X-Z) loading conditions (GK_2, GK_6, GK_{10}, GK_{15}) of the Wenchuan-Tangyu wave are selected for seismic dynamic response analysis.

Figure 3   Loose body stripping stage

Figure 4   Development stage of local earthquake damage

Figure 5   Whole failure stage

3. 1   Analysis about Time Peak of Acceleration

Fig.6 shows the time when the acceleration response of GK_6 slope reaches the peak value. With the increase of slope elevation, the time when the acceleration of X-direction and Z-direction reaches their peak values presents an opposite trends. The peak acceleration time in X-direction shows an advanced trend with the increase of elevation, while thethat of Z-direction presents a delayed trend with the increase of elevation. In addition, the peak

acceleration time of different directions at the same position is not consistent. It can be considered that the transmission of the horizontal seismic waves in rock and soil has greater influence on its internal structure, and the farther away from the seismic source, the less similarity between the acceleration response time curve and the input seismic wave time curve. On the contrary, the vertical seismic wave transmission has less influence on the soil structure, and the similarity between the acceleration response time curve and the seismic wave time curve is higher. Therefore, with the increase of the distance from the seismic source, the time of peak acceleration corresponding to the input seismic wave will be further delayed.
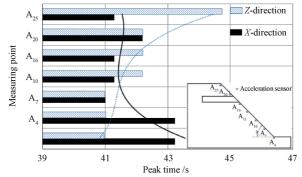

Figure 6　Time Chart of peak acceleration of slope surface

3.2　Analysis of Acceleration Variation against Slope Elevation

We select the acceleration sensors A_4, A_7, A_{10}, A_{11}, A_{16}, A_{20}, A_{25} to draw the relation curve between the peak acceleration and slope elevation. From Fig.7, we can obtain the following information. Firstly, both horizontal and vertical peak acceleration increase with the increase of shaking table load. Secondly, by analyzing the variation rules of the peak acceleration of the tunnel soil, we can conclude that before the stable stage and the loose body stripping stage (GK_{10}), the peak acceleration difference between the tunnel vault and inverted arch area is small. After entering into the development stage of local earthquake damage and the whole failure stage of the model, the nonlinear response of slope acceleration is prominent, the curve decreases obviously at the vault of the tunnel, but increases obviously at the inverted arch. The acceleration response in the vault and inverted arch areas shows an opposite varying trend, and the peak values present a "staggered peak distribution". Furthermore, the vertical acceleration has a more strikingly violent change. According to the tunnel failure situation, the bottom of inverted arch area at the portal section subsides. Therefore, the "staggered peak distribution" phenomenon of the maximum acceleration values at the vault and inverted arch area can be considered as a criterion indicating that the tunnel enters into the threshold of dynamic failure.

3.3　Variation Rules of Peak Ground Acceleration and Coefficient of Amplification

We summarize the variation rules of peak ground acceleration (PGA) and the PGA amplification factor of vault and inverted areas with the change of shaking table acceleration, as shown in Figs.8-9. Among them, PGA amplification factor is defined as the ratio of the peak acceleration of A_{16} and A_{20} in vault and inverted arch areas to the peak acceleration of A_4 measuring point at the slope bottom.
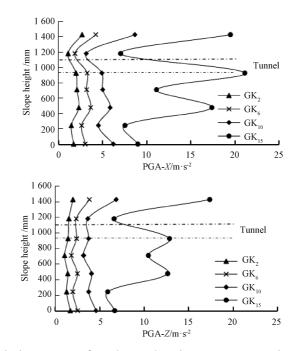
Figure 7 Variation curve of peak acceleration response against slope elevation
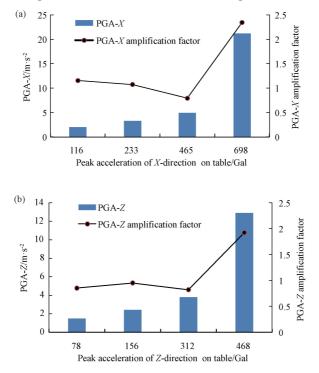（a）Horizontal peak acceleration curve；（b）Vertical peak acceleration curve

Figure 8 Relationship curve between PGA in the inverted arch area and the PGA of shaking table
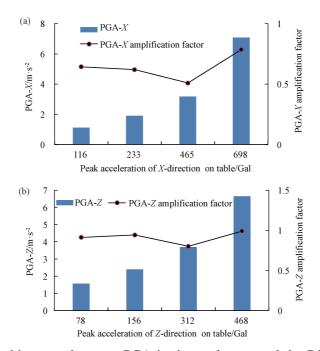（a）PGA-X of the inverted arch area；（b）PGA-Z of inverted arch area

Figure 9   Relationship curve between PGA in the vault area and the PGA of shaking table
（a）PGA-X of the vault area；（b）PGA-Z of the vault area

It can be seen from Fig. 8 and Fig. 9 that the variation trend of the PGA and PGA amplification factor is different. The PGA trend increase linearly before the development stage of local earthquake damage, and then increases suddenly in the whole failure stage of the slope, while the variation trend of the PGA amplification factor generally shows a decreasing trend in the development of local earthquake damage and the previous stages. The main reason is that the slope has a shear-out trend at the toe of the slope, in which the soil is relatively loose compared with the soil in the upper part of the slope during the vibration process. Furthermore, the data obtained by the accelerometer are relatively large, leading to a decreasing trend of the PGA amplification coefficient.

After entering into the whole failure stage, the PGA amplification factor becomes consistent with that of PGA, and both of them increase suddenly, mainly due to the failure of soil around the tunnel. Therefore, the PGA amplification factor response of the slope is related to the failure state of the slope, which is not only associated with its own physical mechanics and geometric shape（internal factors）（Liu Jia et al., 2009）, but the intensity of seismic waves（external factors）（Xu Guangxing et al., 2008）. Therefore, the characteristics of slope and seismic wave intensity are two important factors affecting the variation of PGA amplification factor.

3.4   Variation Analysis of the Acceleration Along Tunnel Depth

Fig. 10 shows that the acceleration response dose not decrease with the increase of tunnel depth when the input seismic intensity is small. At this time, the tunnel is still in the stage of linear dynamic response. The main reason is that the overburden soil layers of the shallow-buried tunnel is thin; moreover, the enlargement effect of the portal section is not obvious caused by the free surface effect of the slope surface. When the input seismic

intensity increases, the tunnel enters into the nonlinear failure stage, the amplification effect of the portal section becomes more obvious. The joint is located at a depth of 50 cm in the tunnel, where the varying trend of the acceleration in the inverted arch area and the vault area is opposite. The acceleration value in the vault area is far greater than that in the inverted arch area. At this stage, the tunnel is broken at the joints, t showing a "staggered peak distribution" pattern.
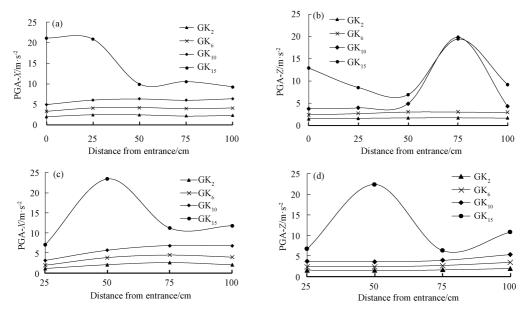

Figure 10   The relationship between peak ground acceleration and tunnel depth
(a) PGA-X of the inverted arch area; (b) PGA-Z of the inverted arch area;
(c) PGA-X of the vault area; (d) PGA-Z of the vault area

4   ANALYSIS OF THE PRESSURE REPONSE OF SURROUNDING ROCK

Fig.11 shows the distribution of soil pressure along the tunnel depth at the vault and inverted arch area. The curve above the X-axis indicates that the soil pressure of the measuring point is greater than the static soil pressure; on the contrary, the curve below the X-axis indicates that the soil pressure at the measuring point is less than the static soil pressure. The variation rules of soil pressure on the inverted arch and vault area along the depth of the tunnel also presents the pattern of "staggered peak distribution".

It can be seen from Fig.11 that the soil pressure increases at the point 50 cm to the inverted arch area, while the soil pressure at the vault changes slightly. Moreover, the point 50 cm to the inverted arch area is also the joint position of the tunnel, which belongs to the weak section. Thus, we infer that the bending occurs at the point. Combined with the subsidence phenomenon in the portal section of the tunnel during the whole failure stage, the overall deformation schematic diagram of the tunnel is summarized as shown in Fig.12.
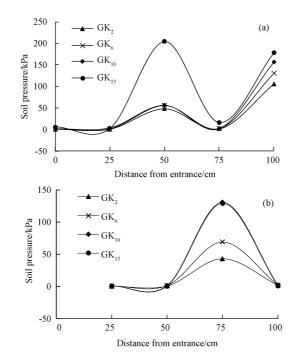
Figure 11　The relationship curve between peak soil pressure and tunnel depth
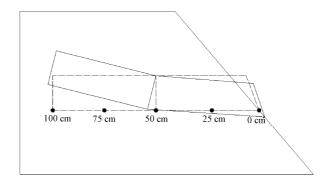（a）Soil pressure at the inverted arch area；（b）Soil pressure at the vault area

Figure 12　Schematic diagram of tunnel deformation

5　CONCLUSION

This study analyzes the failure mode, acceleration response and surrounding rock pressure response of the shallow-buried loess tunnel model under the load generated by earthquakes. Main conclusions are obtained as follows：

（1）The failure process of shallow-buried loess tunnel and slope model traversing high loess slope under seismic load is summarized into four stages, which are "stable stage, loose body stripping stage, local earthquake damage development stage, and whole failure stage".

（2）The "staggered peak distribution" phenomenon of the peak acceleration values at

the vault and inverted arch areas is proposed as a criterion which indicates that the tunnel enters into the threshold of dynamic failure.

（3）Due to the insufficient constraint of the overburden soil layers on the shallow-buried loess tunnel under the effect of earthquakes, the free surface effect of the slope surface may exert great influence on the overall anti-seismic performance of the tunnel, leading to weak earthquake resistance ability. The acceleration, soil pressure and typical failure characteristics of the tunnel joints indicate that the expansion joints, settlement joints and working joints of a tunnel are the key parts for seismic resistance.

ACKNOWLEDGMENT

REFERENCES

Geng Ming. The numerical analysis and experimental study on tunnel structure under seismic ground motion［D］. Chongqing：Chongqing Jiaotong University, 2014（in Chinese with English abstract）.

Guo Zihong, Luo Ruyue, Li Tangyong, Zou Gaoqiang, Yang Tao. Shaking table test for seismic damage of shallow tunnel subjected to incremental loading in soft surrounding rock ［J］. *Chinese Journal of Underground Space and Engineering*, 2019, 15(4): 1081-1090 （in Chinese with English abstract）.

Hashash Y. M. A., Hook J. J., Schmidt B., Yao J. I. C. Seismic design and analysis of underground structures［J］. *Tunnelling and Underground Space Technology*, 2001, 16 (4): 247-293.

Jiang Shuping, Fang Lin, Lin Zhi. Seismic response analysis of mountain tunnels in different depths［J］. *Rock and Soil Mechanics*, 2014, 35(1): 211-216, 225（in Chinese with English abstract）.

Jiang Yitao, Xu Xiuli, Wei Jun, et al. Propagation characteristics of ground motion in shallow tunnel site［J］. *Journal of Nanjing University of Technology（Natural Science Edition）*, 2016, 38(3): 87-93（in Chinese with English abstract）.

Li Lin, He Chuan, Geng Ping, Cao Dongjie. Study of shaking table model test for seismic response of portal section of shallow unsymmetrical loading tunnel［J］. *Chinese Journal of Rock Mechanics and Engineering*, 2011, 30(12): 2540-2548（in Chinese with English abstract）.

Li Tianbin. Failure characteristics and influence factor analysis of mountain tunnels at epicenter zones of great Wenchuan earthquake［J］. *Journal of Engineering Geology*, 2008, 16(6): 742-750（in Chinese with English abstract）.

Li Xiaoyun. The response characteristic research of shallow-tunnel timbering structure under earthquake load［D］. Xi'an: Xi'an University of Science and Technology, 2011（in Chinese with English abstract）.

Liang Qingguo, Bian Lei, Zhang Qinpeng, Huang Jun, Wang Meng. Study on seismic dynamic characteristics of large section loess tunnel portal［J］. *Journal of Highway and Transportation Research and Development*, 2018, 35（7）: 65－76（in Chinese with English abstract）.

Liu Jia, Lu Hai, Cui Yinghui, Lü Ji. Research on stability of slopesd under dynamic forces

［J］. *Journal of North China University of Technology*, 2009, 21(1)：90−94 (in Chinese with English abstract).

Lou Kangyu. Study on the full curve of the stress− strain relationship for microconcrete under compression［D］. Shanghai：Tongji University, 1988 (in Chinese).

Wang Lanmin, Pu Xiaowu, Chen Jinchang. Distribution feature and disaster risk of earthquake-induced landslide in Loess Plateau［J］. *City and Disaster Reduction*, 2019(3)：33−40 (in Chinese with English abstract).

Wang Lili, Wu Zhijian, Liang Qingguo, Sun Wen, Wang Huijuan. Influence of slope gradient on dynamic response in portal section of tunnel［J］. *China Earthquake Engineering Journal*, 2016, 38(4)：519−524 (in Chinese with English abstract).

Wang Mingnian, Lin Jinguo, Yu Li, Cui Guangyao. *Tunnel Seismic and Shock Absorption*［M］. Beijing：Science Press, 2012 (in Chinese)

Wang W.L., Wang T.T., Su J.J., Lin C.H., Seng C.R., Huang T.H. Assessment of damage in mountain tunnels due to the Taiwan Chi-Chi earthquake ［J］. *Tunnelling and Underground Space Technolog*y, 2001, 16(3)：133−150.

Wang Zhengzheng, Gao Bo, Jiang Yuanjun, Yuan Song. Investigation and assessment on mountain tunnels and geotechnical damage after the Wenchuan earthquake［J］. *Science in China Series E：Technological Sciences*, 2009, 52(2)：546−558.

Xu Guangxing, Yao Lingkan, Li Zhaohong, Gao Zhaoning. Dynamic response of slopes under earthquakes and influence of ground motion parameters ［J］. *Chinese Journal of Geotechnical Engineering*, 2008, 30(6)：918−923 (in Chinese with English abstract).

Yuan Shuai. Seismic Response analysis of shallow-depth tunnel and vibration absorption measure［D］. Wuhan：Wuhan University of Technology, 2008 (in Chinese with English abstract).

Zhang Hong, Xu Bin, Liu Youping, Zhu Haiqin. Analysis on the seismic dynamic response and shock-absorption measures of the layered saturated soil embedded a lining subjected to seismic wave［J］. *Chinese Journal of Underground Space and Engineering*, 2016, 12 (S2)：856−862 (in Chinese with English abstract).

Zhu Yongsheng. Numerical analysis and study on seismic response of shallow-depth tunnel［D］. Chengdu：Southwest Jiaotong University, 2006 (in Chinese).

About the Author

SUN Wen, born in 1987, is a Ph.D. student at Lanzhou Jiaotong University. He is mainly engaged in geotechnical and underground enginnering. E-mail：154310011@ qq.com

Corresponding author：LIANG Qingguo, born in 1976. is a professor at Lanzhou Jiaotong University. His major engaged in geotechnical and underground engeering.E-mail：lqg_39@ 163. com